

Role of S/Se ratio in chemical bonding of As–S–Se glasses investigated by Raman, x-ray photoelectron, and extended x-ray absorption fine structure spectroscopies

Wenyan Li^{a)} and Sudipta Seal

Advanced Materials Processing and Analysis Center and Mechanical, Materials and Aerospace Engineering Department, University of Central Florida, Orlando, Florida 32816

Clara Rivero, Cedric Lopez, and Kathleen Richardson

Center for Research and Education in Optics and Lasers, College of Optics and Photonics, University of Central Florida, Orlando, Florida 32816

April Pope and Alfons Schulte

Department of Physics, University of Central Florida, Orlando, Florida 32816

Satish Myneni

Department of Geosciences, Princeton University, Princeton, New Jersey 08544

Himanshu Jain and Keisha Antoine

Department of Materials Science and Engineering, Lehigh University, Bethlehem, Pennsylvania 18015

Alfred C. Miller

Zettlemoyer Center for Surface Studies, Lehigh University, Bethlehem, Pennsylvania 18015

(Received 15 November 2004; accepted 6 July 2005; published online 2 September 2005)

Chalcogenide glasses have attracted considerable attention and found various applications due to their infrared transparency and other optical properties. The As–S–Se chalcogenide glass, with its large glass-formation domain and favorable nonlinear property, is a promising candidate system for tailoring important optical properties through modification of glass composition. In this context, a systematic study on ternary As–S–Se glass, chalcogen-rich versus well-studied stoichiometric compositions, has been carried out using three different techniques: Raman spectroscopy, x-ray photoelectron spectroscopy, and extended x-ray absorption fine structure spectroscopy. These complementary techniques lead to a consistent understanding of the role of S/Se ratio in chalcogen-rich As–S–Se glasses, as compared to stoichiometric composition, and to provide insight into the structural units (such as the mixed pyramidal units) and evidence for the existence of homopolar bonds (such as Se–Se, S–S, and Se–S), which are the possible structural origin of the high nonlinearity in these glasses. © 2005 American Institute of Physics. [DOI: [10.1063/1.2009815](https://doi.org/10.1063/1.2009815)]

I. INTRODUCTION

Chalcogenide glasses have attracted considerable attention due to their infrared transparency, low phonon energies, and high nonlinear optical properties.^{1–5} They have been explored as promising materials for optical memories, grating, and switching devices.^{6–10} Recently these glasses are used as core materials for high-efficiency fiber amplifiers as they exhibit high refractive indices and low phonon energies,^{11–15} and as candidate for Raman gain media.¹⁶

Among chalcogenide glasses, the As–S–Se system is characterized by a large glass-formation domain¹⁷ and favorable nonlinear properties,⁴ as well as their linear properties. The wide range of glass formation makes this glass system an ideal candidate for tailoring important optical properties through modification of glass composition.⁴ The ease of glass formation makes it desirable for low-loss optical applications. In this context, studies of chemical and structural properties of As–S–Se glasses with different composition are

important for understanding their optical behavior. A systematic study on ternary As–S–Se glass, chalcogen-rich versus well-studied stoichiometric compositions, has been carried out, and the results are reported in this paper. The interest in chalcogen-rich compositions is due to the high nonlinearity found in $\text{As}_{24}\text{S}_{38}\text{Se}_{38}$, which possesses a third-order nonlinearity of 400 times that of silica.⁴

In previous studies, different techniques have been used to understand the structure of chalcogen glasses. Three of them have been proven very effective: Raman spectroscopy, x-ray photoelectron spectroscopy (XPS), and extended x-ray absorption fine structure spectroscopy (EXAFS), to study various chalcogenide glass systems.

Raman spectroscopy has been used to study bulk S–Se, As–S, and As–Se systems,^{18–25} as well as evaporated chalcogenide films of As_2Se_3 and As_2S_3 , which showed significantly different bonding as compared with bulk quenched glasses.²⁶ Our previous study²⁷ also revealed significant microstructural difference between unannealed films and fibers drawn from bulk As_2S_3 glasses.

XPS has been used to study the electronic structure of

^{a)}Author to whom correspondence should be addressed; electronic mail: Wenyan.Li-1@ksc.nasa.gov

chalcogenides,^{28–31} as well as photoinduced structural changes such as photodecomposition,³² oxidation,^{33,34} and other compositional changes.³⁵ *In situ* XPS has also been applied to the study of light-induced changes in As–Se glasses.^{36,37} In our previous studies, XPS has been employed to describe the structural changes in As₂S₃ caused by different energy beams³⁸ and also the chemical stability of chalcogenide glass under elevated temperatures.³⁹

EXAFS is a powerful tool for a detailed and quantitative understanding of the local atomic structure of amorphous materials.^{26,40–49} X-ray absorption spectroscopy (XAS) has been used to study arsenic chalcogen binary compounds and a few compositions in the As–S–Se system.^{44,50,51} A comparison of theoretically and experimentally determined bond strength and chemical order was made in As_xS_{1–x}, for bulk as well as for film.^{43,44,52,53} EXAFS has also been used to study the photodarkening in amorphous As₂S₃.^{54,55} The photoinduced formation of dynamical bonds has been observed in amorphous Se by *in situ* EXAFS.^{56,57,14} Both experimental and theoretical studies have been carried out in As–Se binary glassy system,^{15,58,59} indicating photoinduced Se-related structural changes.

Most previous works have been carried out in arsenic chalcogen binary compounds, and the results¹⁸ have been interpreted in terms of pyramidal subunits, using the well-accepted molecular model for As₂(S,Se)₃ glasses proposed by Lucovsky and Martin.⁶⁰ However, the model only predicts vibrational modes for ideal, stoichiometric As₂(S,Se)₃ glass compositions, it does not account for modes associated with abnormal bonding configurations (e.g., homopolar bonds or chalcogen-chalcogen bonds) known to be present in stoichiometric compositions in small amount, and which are also potentially important configurations found in chalcogen-rich As–S–Se system.⁴

In this paper, we present the findings of a study on the role of S/Se ratio in As–S–Se glasses using Raman XPS, and EXAFS. Raman provides bonding information about different structural groups. XPS provides information on the chemical environment of the three elements as well as the valence band. Through EXAFS, one can gain quantitative information on the atoms' nearest neighbors, including bond length and coordination numbers. This paper aims to explain the variation in S/Se environment in chalcogen-rich As–S–Se glasses, as compared to stoichiometric composition, and to provide insight into the possible existence of abnormally coordinated species (wrong bonds) in these materials.

II. EXPERIMENTAL PROCEDURE

A. Sample preparation

Material compositions were selected from As–S–Se ternary diagram with fixed As content and varying the S/Se ratio (Fig. 1). This study has focused on glasses with chalcogen-rich compositions (6–10 on the diagram) and the variation of their structures and properties, as compared to stoichiometric compositions, 1–5.

Bulk chalcogenide glass (ChG) samples were prepared by conventional melt quenching in evacuated silica ampoules, using the techniques detailed in Ref. 4. Annealed

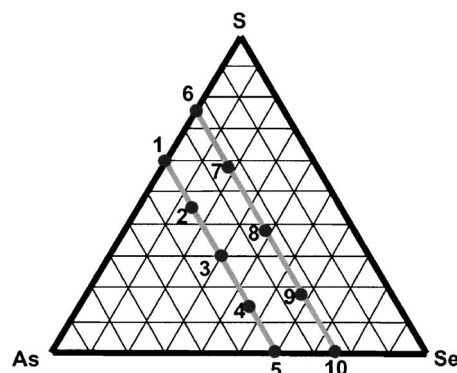


FIG. 1. The ternary composition diagram of the As–S–Se system. The compositions on the diagram is as follows (mol %): (1) As₄₀S₆₀, (2) As₄₀S₄₅Se₁₅, (3) As₄₀S₃₀Se₃₀, (4) As₄₀S₁₅Se₄₅, (5) As₄₀Se₆₀, (6) As₂₄S₇₆, (7) As₂₄S₅₇Se₁₉, (8) As₂₄S₃₈Se₃₈, (9) As₂₄S₁₉Se₅₇, and (10) As₂₄Se₇₆.

ChG samples were removed from the ampoule, cut, ground, and polished using a Buehler polishing machine. The bulk sample size was 10 mm in diameter, nominally 2 mm in average thickness. For XPS experiments, the bulk samples were resized (cut and polished) to 15 × 5 × 1.5 mm³ and fractured inside the ultrahigh vacuum chamber of the spectrometer. The composition of bulk samples was verified by energy dispersive x-ray spectroscopy (X-EDS) built in a JEOL 6400F SEM EDS. The composition error was found to be around or less than 1 mol %.

B. Raman analysis

High-resolution (1.5 cm^{−1}) Raman spectra on bulk As–S–Se glasses were measured using near-infrared excitation to avoid photoinduced changes in these glasses. Raman scattering was excited at 840 nm with a Ti:sapphire laser (30–50 mW) employing a setup described previously.^{61,62} The scattered Raman light was analyzed with a single-grating spectrograph (Instruments SA, HR 640) equipped with a charge-coupled device (CCD) detector (Princeton Instrument).

C. XPS analysis

Bulk glass samples were examined using a Scienta 300 ESCA (Zettlemoyer Center for Surface Studies, Lehigh University) at a vacuum of $\sim 10^{-9}$ Torr. A monochromatic Al K α x-ray source was used for the analysis; a low-energy electron flood gun was used for charge compensation. Both survey scan and individual high-resolution scans were recorded at a pass energy of 150 V. First, As–S–Se bulk glass samples were fractured inside the XPS vacuum chamber, and data were collected on freshly generated surfaces. Core levels, including As3*d*, Se3*d*, and S2*p* (overlapping with Se3*p* in ternary glasses), Auger lines, and valence-band data were collected. Then the fractured surfaces were coated with a thin layer (about 2 nm) of gold inside the preparation chamber, and the spectra of Au4*f* and As and Se (when available) core-level spectra were collected. The Au4*f*_{7/2} line was used as charge reference at 84.00 eV. The “true” binding energy of the As3*d* spectra of the gold-coated sample were obtained

TABLE I. Raman data fitting parameters (peak position and peak width both in wave number) and peak assignments.

Peak position (Wave number, cm^{-1})	Width (Wave number, cm^{-1}) (Gaussian/Lorentzian)	Peak assignment
212	14.5/0.007	Interaction of the AsSe_3 pyramids
227	19.6/10.3	As–Se vibration in AsSe_3 pyramidal units
241	16/1	As–Se vibration in AsCh_3 units and/or Se–Se chain
257	15.87/9	As–Se vibration in AsCh_3 units and/or Se–Se ring fracture
269	18/1.5	Interaction of the AsSe_3 pyramids
312	24.3/5.65	Interaction of the AsSe_3 pyramids
340	30/10.7	As–S vibration in AsSe_3 pyramidal units
362	17/9.8	As–S vibration in AsCh_3 units or interaction between AsSe_3 and S–S chain (~ 365)
380	30/7.85	Interaction of the AsSe_3 pyramids

using $\text{Au}4f_{7/2}$ as a reference, then all the spectra of fresh-fractured glass surface (before Au coating) were charge-corrected using $\text{As}3d$ as a reference.

D. EXAFS analysis

Bulk glass samples were grounded to fine powder for EXAFS experiments. EXAFS data were collected at the Stanford Synchrotron Radiation Laboratory on Beamline 2-3 using $\text{Si}(220)$ monochromator crystals. The slits in front of the monochromator were set at 1.5×14 mm, and the Beamline was detuned by about 50% above the absorption edge. The data were collected at the As edge in both transmission and fluorescence modes; they were compared and found to be identical.

E. Data analysis

1. Raman

The Raman data were fitted with the GRAMS software, using Voigtian curves appropriate for glasses, which allows one to choose the peak center, height, Gaussian width, and Lorentzian width. The Voigt function is a convolution of both the Gaussian and Lorentzian functions. GRAMS peak fitting uses the Levenberg-Marquardt method.⁶³ This is an iterative method that starts with a set of initial values for the peak parameters and modifies them until the variation in the χ^2 value, which measures the goodness of the fit, reaches a specified minimum.

These parameters can be set constant or allowed to vary over a range of values. Each composition was fit initially with a minimal set of values. This allowed the software to assign values to optimize the curve-fitting result. Determination of the peak location of each vibrational band was based on previous literature, which allowed for a precise location to be assigned to each band. Once determined, the peak positions were set constant, and the fitting was carried out again. Then for each band the Lorentzian and Gaussian widths were compared over each composition. These values were then averaged and the mean value was used as a constant parameter in additional fits. At this point only the height was allowed to vary, which also determined the area of each

band and gave the final fitting results. Raman fitting parameters and peak assignment are listed in Table I.

2. XPS

The charge-corrected spectra were analyzed using ESCA Analysis, the XPS data analysis software designed for Scienta ESCA 300 system. As mentioned above, the XPS spectra were charge-corrected using Au coating as reference; then the data were prepared for peak fitting through smoothing and baseline subtraction. Minimal data smoothing was needed due to the good resolution of Scienta ESCA 300 system; Shirley baseline^{64–66} was used for background removal, and the peak ranges were chosen carefully and consistently for different glass compositions. Due to the same reason stated in Sec. II E 1, Voigtian peaks were chosen to carry out peak fitting for each core-level spectrum. First, $\text{As}3d$, $\text{Se}3d$, $\text{S}2p$, and $\text{Se}3p$ peaks were deconvolved into two-parameter Voigtian peaks, using the parameters in Table II, where Δ is the doublet separation for d or p orbitals; DR is the area ratio for the doublets, such as $3d_5/3d_3$ or $2p_3/2p_1$; FWHM is the full width at half maximum of the peaks, and Mix is the Gaussian/Lorentzian mix factor of the peak. The parameters were chosen by using pure elemental data as reference and fitting optimization. As the parameters were chosen, the spectra were fitted with as few peaks as possible. Then through self-consistency of all fitting results and our understanding of the glass system, we assigned the peaks to different chemical environments.

TABLE II. XPS data fitting parameters: Δ is the doublet binding energy separation for p or d orbitals, DR is the area ratio for the doublets, FWHM is the full width at half maximum of the peaks, and Mix is the Gaussian/Lorentzian mix factor of the peaks.

	Δ (eV)	DR	FWHM (eV)	Mix
$\text{As}3d$	0.694	0.71	0.69	0.87
$\text{Se}3d$	0.85	0.76	0.75	0.93
$\text{Se}3p$	5.72	0.41	1.97	0.6
$\text{S}2p$	1.185	0.505	0.77	0.87

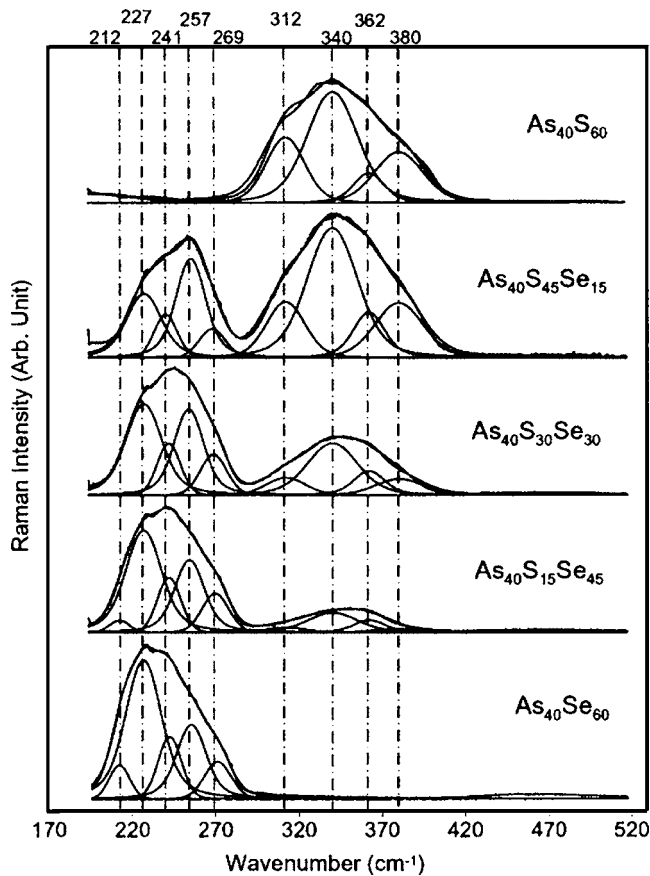


FIG. 2. Raman spectra and deconvolution of bulk chalcogenide glasses $\text{As}_{40}\text{S}_{60-x}\text{Se}_x$.

3. EXAFS

A standard procedure was followed to analyze the EXAFS data.⁶⁷ It began with a theoretical calculation of the scattering amplitudes and phase-shift functions of the As–As, As–Se, As–S, Se–Se, and Se–S pairs from As metal,⁶⁸ $c\text{-As}_2\text{Se}_3$,⁶⁹ $c\text{-As}_2\text{S}_3$,⁷⁰ Se metal, and $c\text{-Se}_5\text{S}_3$, respectively, using the FEFF program.⁷¹ The fitting of the theoretical EXAFS function to the experimental signal was performed in r (or k) space, using EXAFSPAK XAS software package developed by George at Stanford Synchrotron.⁷²

III. RESULTS

A. $\text{As}_{40}\text{S}_{60-x}\text{Se}_x$ glasses ($x=0, 15, 30, 45, 60$)

1. Raman results

Figure 2 depicts the Raman spectra of chalcogenide stoichiometric ternary compounds $\text{As}_{40}\text{S}_{60-x}\text{Se}_x$, where $x=0, 15, 30, 45, 60$ (compositions 1, 2, 3, 4, and 5 in Fig. 1). In all cases, $\lambda_{\text{excitation}}=840$ nm. The peak-fitting results are also shown in the same figure, and will be discussed later.

The dominant features are two broad bands located at 200–280 and 275–400 cm^{-1} . The relative intensity of the two bands changes monotonically with increasing x . As the Se content (x value) increases, the peak of the scattering intensity in the region 200–280 cm^{-1} moves toward lower frequencies. Another change observed in the spectra is that the small shoulders at ~ 210 and ~ 275 become weaker and finally disappear with decreasing Se. The peak shift in the

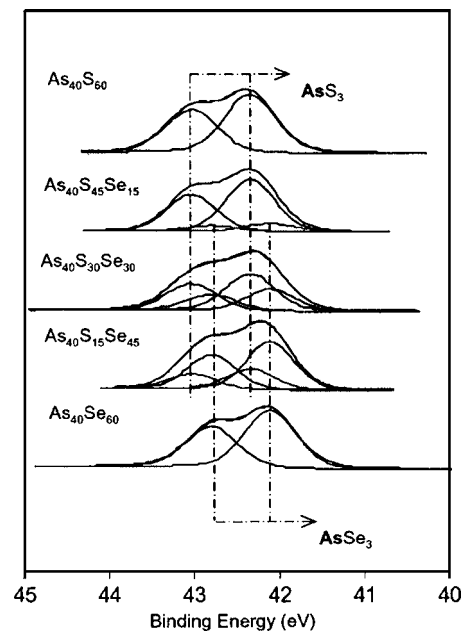


FIG. 3. XPS $\text{As}3d$ spectra and deconvolution of bulk chalcogenide glasses $\text{As}_{40}\text{S}_{60-x}\text{Se}_x$.

280–400 cm^{-1} is less observable, but the two shoulders at 312 and 380 cm^{-1} also reduce in intensity and eventually disappear with increasing Se.

2. XPS results

XPS results of $\text{As}3d$, $\text{Se}3d$, $\text{S}2p$ and $\text{Se}3p$ and the valence band spectra of $\text{As}_{40}\text{S}_{60-x}\text{Se}_x$ bulk glasses are plotted in Figs. 3–6, respectively. The corresponding peak-fitting results are also shown in the same figures, and will be discussed later.

From the $\text{As}3d$ spectra (Fig. 3), we observe that in $\text{As}_{40}\text{S}_{60-x}\text{Se}_x$, with Se increasing from 0 to 60 mol %, the binding energy of $\text{As}3d_{5/2}$ decreases from 42.34 ($\text{As}_{40}\text{S}_{60}$) to 42.11 eV ($\text{As}_{40}\text{Se}_{60}$). The decrease is small, yet well above the experimental uncertainty, which is 0.05 eV. Figure 4 shows a small decrease in the binding energy of $\text{Se}3d_{5/2}$ peak from 53.84 ($\text{As}_{40}\text{S}_{45}\text{Se}_{15}$) to 53.93 eV ($\text{As}_{40}\text{Se}_{60}$) as the Se content increases from 15 to 60 mol %. Figure 5 shows $\text{S}2p$ and $\text{Se}3p$ spectra. The $\text{S}2p$ peaks are located around 162–163 eV, with a separation of 1.18 eV between $\text{S}2p_{3/2}$ and $\text{S}2p_{1/2}$; $\text{Se}3p$ peaks are located in the range of 160–166 eV, with a separation of 5.75 eV between $\text{Se}3p_{3/2}$ and $\text{Se}3p_{1/2}$. As can be seen for the ternary chalcogenide glasses, $\text{Se}3p_{3/2}$ overlaps with the two peaks of $\text{S}2p$. The increase of relative intensity of $\text{S}2p$ peaks with increasing S content is clearly visible. Figure 6 represents the valence-band XPS spectra of $\text{As}_{40}\text{S}_{60-x}\text{Se}_x$ glasses. For comparison, the valence band of elemental Se sample is also shown. There is a relatively small variation of the valence-band structure among the different $\text{As}_{40}\text{S}_{60-x}\text{Se}_x$ glasses. It can be noticed that the band at 5.5 eV remains featureless. A band in this region is characteristic of elemental Se.

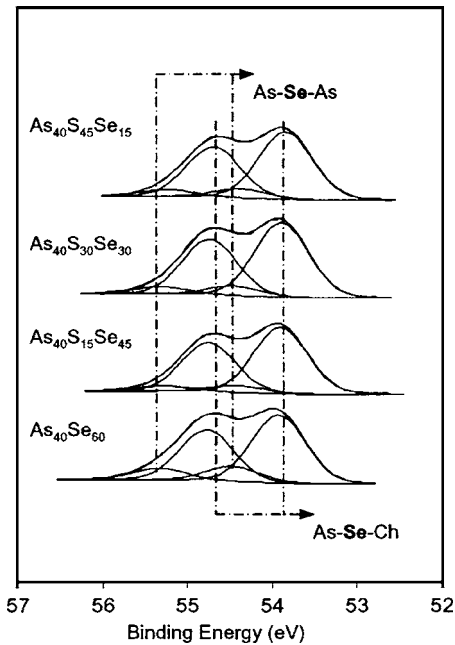


FIG. 4. XPS $Se3d$ spectra and deconvolution of bulk chalcogenide glasses $As_{40}S_{60-x}Se_x$.

B. $As_{24}S_{76-x}Se_x$ glasses ($x=0, 19, 38, 57, 76$)

1. Raman results

Figure 7 depicts the Raman spectra of bulk chalcogen-rich glasses $As_{24}S_{76-x}Se_x$ ($x=0, 19, 38, 57, 76$), which correspond to compositions 6, 7, 8, 9, and 10 in Fig. 1. The peak-fitting results are also shown in the same figure, and will be discussed later.

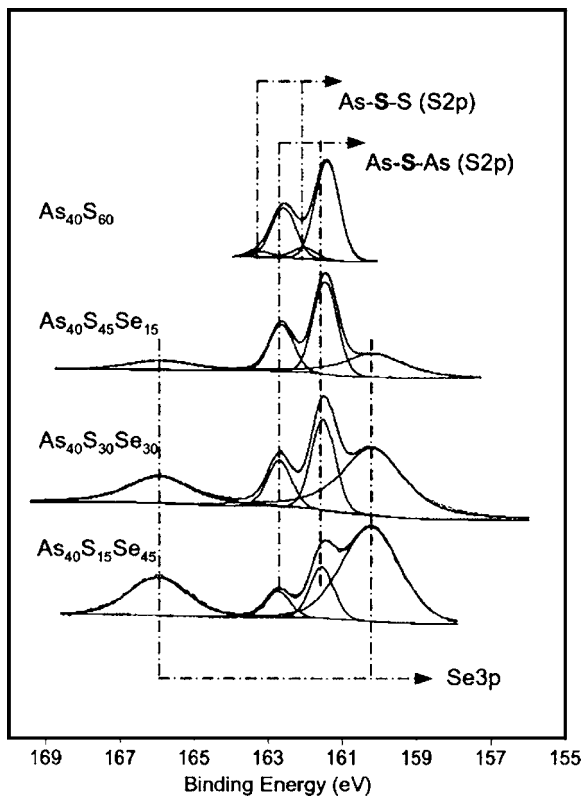


FIG. 5. XPS $S2p$ and $Se3p$ spectra and deconvolution of bulk chalcogenide glasses $As_{40}S_{60-x}Se_x$.

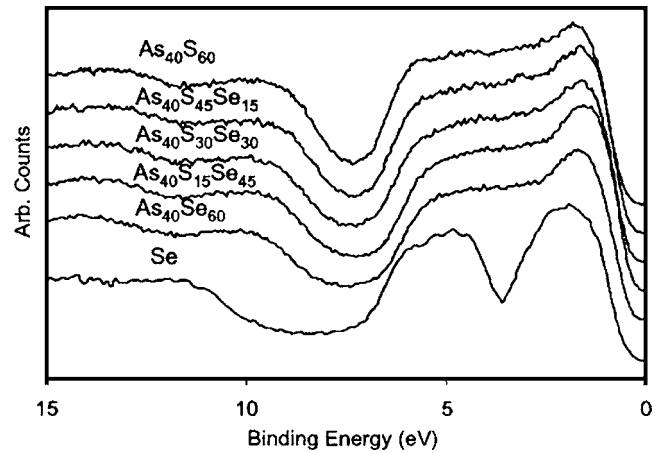


FIG. 6. Valence bands in $As_{40}S_{60-x}Se_x$ bulk chalcogenide glasses.

As the stoichiometric ternary compounds in $As_{40}S_{60-x}Se_x$ series, there are two broad bands located at similar positions in the Raman spectra for $As_{24}S_{76-x}Se_x$, associated with As-S and As-Se vibrations. However, differences can clearly be seen between the two systems. Firstly, a new band appears at the high-frequency range ($420\text{--}520\text{ cm}^{-1}$) for S-rich $As_{24}S_{76-x}Se_x$, which is accompanied by the rising background in the low-frequency range (below 280 cm^{-1}). Secondly, in As-Se-related range ($200\text{--}280\text{ cm}^{-1}$), there is an emergency of the 257-cm^{-1} peak in every Se-containing $As_{24}S_{76-x}Se_x$ glass. In all the Se-containing $As_{24}S_{76-x}Se_x$ glasses, a noticeable change in the broad band between 200 and 280 cm^{-1} with decreasing Se content is the decrease of the intensity of the band at 227 cm^{-1} , which is characteristic of the As-Se vibration in $AsSe_3$ pyramids.

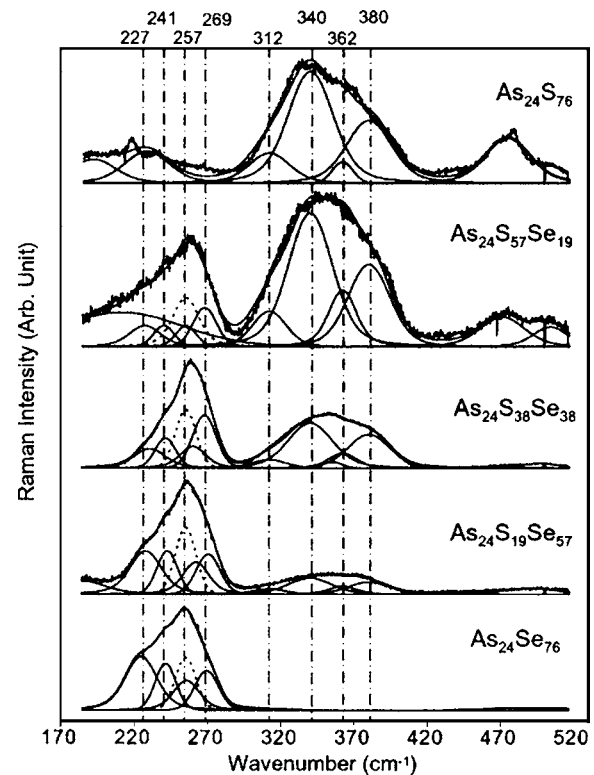


FIG. 7. Raman spectra and deconvolution of bulk chalcogenide glasses $As_{24}S_{76-x}Se_x$.

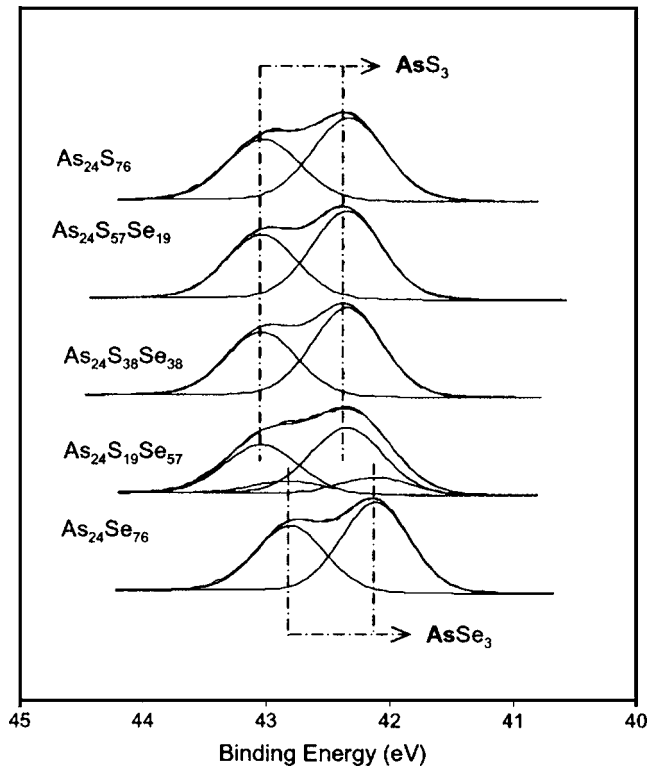


FIG. 8. XPS $As3d$ spectra and deconvolution of bulk chalcogenide glasses $As_{24}S_{76-x}Se_x$.

For $As_{24}S_{76}$, while the 340-cm^{-1} band (As-S in AsS_3) remains strong, the 312-cm^{-1} shoulder is substantially weaker as compared with $As_{40}S_{60}$. Also a shoulder at 365 cm^{-1} appears, which has been assigned to the As_2S_5 structure, and interaction occurs between AsS_3 pyramids with S-S chains.^{73,74} Meanwhile, the two bands at 219 and 474 cm^{-1} , associated with S_8 rings,^{75,18} are also observed. In addition to those peaks, a weak peak at 494 cm^{-1} and a shoulder at 465 cm^{-1} also are observed; the former is associated with S-S chains¹⁸ and the latter has been suggested to be an indication of a terminal, or nonbridging, As-S bond, such as in $AsS_3=S$.⁷³ In $As_{24}S_{57}Se_{19}$, one can observe a slight shift of the As-S band, and the S-S chain (494 cm^{-1}) and S ringlike (474 cm^{-1}) structures are still observable.

2. XPS result

XPS results of $As3d$, $Se3d$, $S2p$ and $Se3p$, and the valence-band spectra of $As_{24}S_{76-x}Se_x$ bulk glasses are plotted in Figs. 8–11, respectively. The corresponding peak-fitting results are also shown in the same figures, and will be discussed later.

From the $As3d$ spectra (Fig. 8), we observe that in $As_{24}S_{76-x}Se_x$, with Se increasing from 0 to 76 mol %, the binding energy of $As3d_{5/2}$ decreases from 42.34 ($As_{24}S_{76}$) to 42.12 eV ($As_{24}Se_{76}$). From $As_{24}S_{76}$ to $As_{24}S_{38}Se_{38}$, the binding energy shows very little change; the variation of binding energy is more clearly observable in the Se-rich compositions. The $As3d$ peak of $As_{24}S_{19}Se_{57}$ is relatively broad, indicative of different As environments. Figure 9 shows a small decrease in the binding energy of $Se3d_{5/2}$ peak from 54.55 to 54.37 eV as the S content decreases; the $Se3d$ peaks

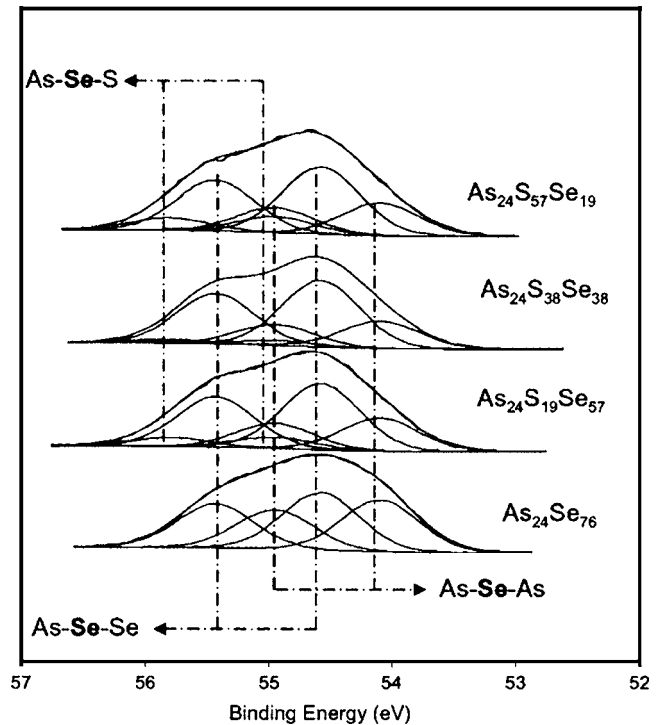


FIG. 9. XPS $Se3d$ spectra and deconvolution of bulk chalcogenide glasses $As_{24}S_{76-x}Se_x$.

for $As_{24}S_{76-x}Se_x$ glasses are wider compared with $As_{40}S_{60-x}Se_x$ glasses, and the $3d$ split is less visible. Both indicate more than one Se environment in $As_{24}S_{76-x}Se_x$ glasses. Figure 10 shows the $S2p$ and $Se3p$ peaks of $As_{24}S_{76-x}Se_x$ glasses. Comparing the $S2p$ peaks of these

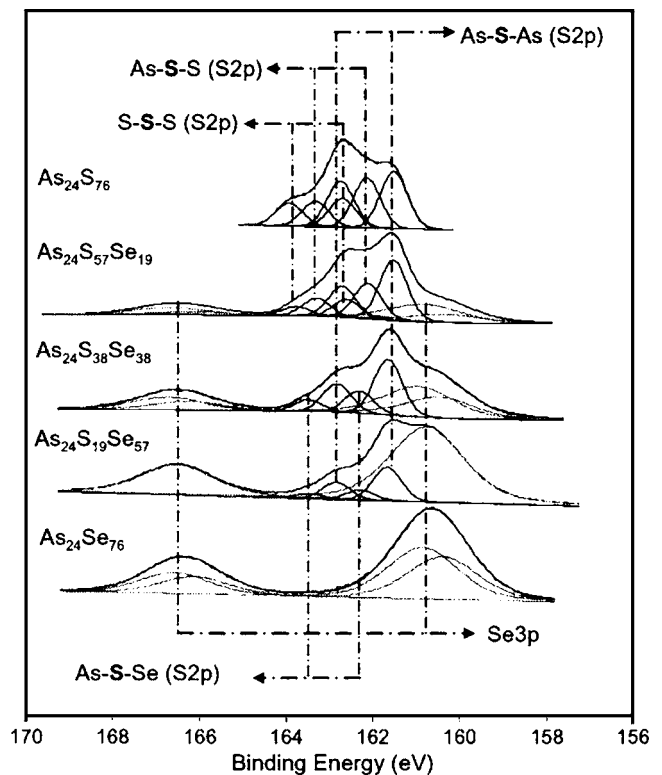


FIG. 10. XPS $S2p$ and $Se3p$ spectra and deconvolution of bulk chalcogenide glasses $As_{24}S_{76-x}Se_x$.

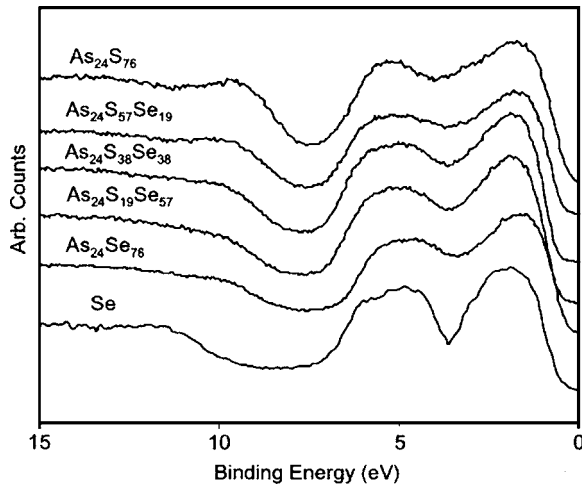


FIG. 11. Valence bands in $\text{As}_{24}\text{S}_{76-x}\text{Se}_x$ bulk chalcogenide glasses.

glasses with that of $\text{As}_{40}\text{S}_{60-x}\text{Se}_x$, it is clear that more than one S environment is present in the chalcogen-rich glasses. Figure 11 represents the valence-band XPS spectra of $\text{As}_{24}\text{S}_x\text{Se}_{76-x}$ glasses. For comparison, the valence band of elemental Se sample is also shown in Fig. 11. With increasing Se, the band located at 5.5 eV becomes more distinct, which are characteristic of elemental Se.

3. EXAFS results

The normalized EXAFS spectra of the arsenic *K* edges for glass compositions in the series $\text{As}_{24}\text{S}_{76-x}\text{Se}_x$ ($x=19, 38, 57$) are shown in Fig. 12(a). The phase-corrected Fourier transformation of arsenic *K*-edge EXAFS spectra for all glass spectra are shown in Fig. 12(b).

For the three compositions measured, the arsenic *K*-edge EXAFS spectra showed a single peak. For the constant arsenic samples, replacing S by Se shifts the peak maximum in the radial distribution function to higher values, which indicates a lengthening of bonds between As and its neighbor. The peak maximum, corresponding to the average bond length, was almost the same for $\text{As}_{24}\text{S}_{57}\text{Se}_{19}$ (2.3 Å) and $\text{As}_{24}\text{S}_{38}\text{Se}_{38}$ (2.29 Å), but a bigger change is noticed in $\text{As}_{24}\text{S}_{19}\text{Se}_{57}$ (2.34 Å). The corrected and fitted data results using the EXAFSPAK XAS software are shown in Table III.

IV. DISCUSSION

A. $\text{As}_{40}\text{S}_{60-x}\text{Se}_x$ glasses ($x=0, 15, 30, 45, 60$)

1. Raman results

Broad bands at 200–280 and 280–400 cm^{-1} have been observed in binary selenide As_2Se_3 and sulfide As_2S_3 , re-

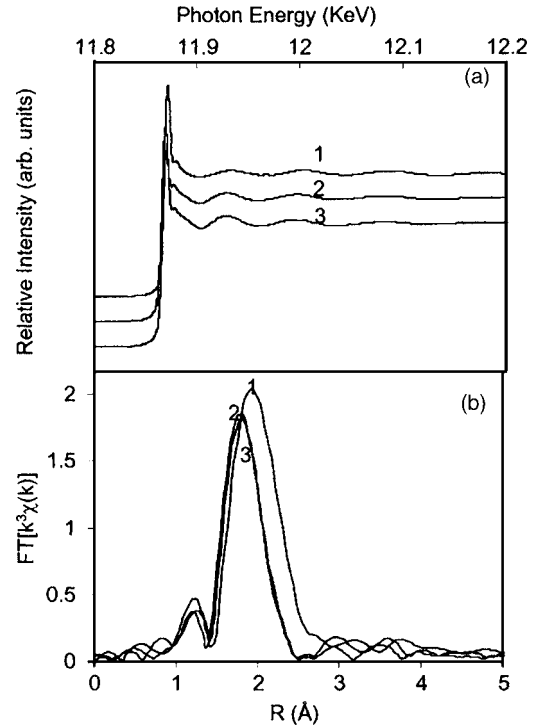


FIG. 12. (a) Arsenic *K*-edge EXAFS spectra and (b) the Fourier-transformed arsenic *K*-edge EXAFS for $\text{As}_{24}\text{S}_{76-x}\text{Se}_x$. Three sample compositions examined include [Fig. 1 composition number]: (1) $\text{As}_{24}\text{S}_{19}\text{Se}_{57}$ [9], (2) $\text{As}_{24}\text{S}_{38}\text{Se}_{38}$ [8], and (3) $\text{As}_{24}\text{S}_{57}\text{Se}_{19}$ [7].

spectively. The former is attributed to As–Se–As stretching vibration in the AsSe_3 pyramids and the latter to As–S–As in AsS_3 pyramids.^{18,23,73,76–86} The relative intensity change of these two broad bands (shown in Fig. 2) is consistent with the change of the relative ratio of Se/S in these glasses.

Similar peak shifts in the As–Se-related band (200–280 cm^{-1}) were also observed by Frietas *et al.*⁸⁷ and Onari *et al.*⁸⁸ The peak shift and the polarization study in the reference suggested that more than one species of vibration is contributing to the band at (200–280 cm^{-1}). There are four possible $\text{AsS}_{3-n}\text{Se}_n$ pyramids with $n=0, 1, 2, 3$. Among them, three pyramids can contribute to As–Se vibration, AsS_2Se , AsSSe_2 , and AsSe_3 . With increasing Se in the pyramids, the mode mass would be expected to be somewhat bigger and, consequently, the frequency would be expected to be lower. This is consistent with the observed frequency shift of the 200–280- cm^{-1} band.

According to Wagner *et al.*,⁷⁴ the two shoulders around 312 and 380 cm^{-1} in the As–S range are due to interactions among and between the AsS_3 pyramids. With increasing Se,

TABLE III. EXAFS data-fitting results: *N*—neighboring atom number; *R*—the distance from neighboring atom to the absorbing atom; σ —the standard deviation of the interatomic distance, and ΔE_0 —correction for estimated edge step E_0 .

Composition	Fitting	Shell	<i>N</i>	<i>R</i> (Å)	σ^2 (Å ²)	ΔE_0 (eV)
$\text{As}_{24}\text{S}_{38}\text{Se}_{38}$	With S	As–S	3.1	2.29	0.0035	–7.4
$\text{As}_{24}\text{S}_{57}\text{Se}_{19}$	With S	As–S	3.31	2.3	0.004	–5.916
$\text{As}_{24}\text{S}_{19}\text{Se}_{57}$	Add Se	As–S	1.92	2.32	0.0004	3.679
		As–Se	2	2.49	0.011	3.679

there are fewer AsS_3 pyramids in the glasses, and the intensity of interaction-related vibration should be reduced. This is consistent with our observation. A similar reason could account for the disappearance of two shoulders in As–Se-related frequency range.

Figure 2 shows the peak deconvolution of the Raman results of $\text{As}_{40}\text{S}_{60-x}\text{Se}_x$ glasses. In the As–Se-related peak range, the main Raman bands are assigned to the As–Se vibration of the AsSe_3 and $\text{AsS}_{3-n}\text{Se}_n$ pyramids (227 , 241 , and 257 cm^{-1}) and their interactions (269 cm^{-1}); and in As–S-related range, the deconvoluted Raman peaks are assigned to the As–S vibration of the AsS_3 and $\text{AsS}_{3-n}\text{Se}_n$ pyramids (340 and 362 cm^{-1}) and their interactions (312 and 380 cm^{-1}). This is consistent with the multiple vibrations found in crystalline As_2Se_3 , As_2S_3 , and As_2SSe_2 .^{87,89} However, we must also point out that the peaks at 241 and 257 cm^{-1} are also the main features in pure Se glasses and they have been assigned for Se–Se vibration in chain and ring fragments, respectively.⁹⁰ Likewise, the peak at 362 cm^{-1} corresponds to the main feature of As_4S_4 molecules.⁹¹ We do not consider that the peak components around 241 and 257 cm^{-1} are evidence of Se–Se bonds in bulk $\text{As}_{40}\text{S}_{60-x}\text{Se}_x$ glasses. To our knowledge, no previous study supports the expectation for a large quantity of Se–Se homopolar bonds in bulk $\text{As}_{40}\text{S}_{60-x}\text{Se}_x$ glasses, although it is possible that a limited amount of Se–Se “wrong” bonds exist in stoichiometric composition, which is confirmed by XPS. As for the 362-cm^{-1} peak component, which has been previously associated with the As_4S_4 molecular clusters in As_2S_3 films^{27,91} and As-rich $\text{As}_x\text{S}_{1-x}$ bulk glasses,⁷⁹ the existence of those peak components does not necessarily indicate the presence of As_4S_4 molecules in $\text{As}_{40}\text{S}_{60-x}\text{Se}_x$ bulk glasses. Actually, the nuclear quadrupole resonance (NQR) study in glassy As_2Se_3 and As_2S_3 systems⁹² of Treacy *et al.* shows that there is no As_4Ch_4 (Ch=S, Se) molecule found in bulk As_2Se_3 and As_2S_3 , while they are the main components in as-deposited films, as shown by previous studies.²⁷

2. XPS results

Figures 3, 4, and 5 show the peak deconvolution of the XPS results of $\text{As}3d$, $\text{Se}3d$, and $\text{S}2p$ for the $\text{As}_{40}\text{S}_{60-x}\text{Se}_x$ series. According to the $\text{As}3d$ peaking-fitting results of $\text{As}_{40}\text{S}_{60-x}\text{Se}_x$ (Fig. 3), the As atoms exist in AsCh_3 units (Ch=S, Se). The $\text{As}3d$ peak is deconvoluted into two components, AsS_3 ($\text{As}3d_{5/2}$ at 42.34 eV) and AsSe_3 ($\text{As}3d_{5/2}$ at 42.11 eV). Note that the complete representation of all possible mixed pyramidal units is using As_2S_3 , $\text{As}_2\text{S}_2\text{Se}$, As_2SSe_2 , and As_2Se_3 components to deconvolute the $\text{As}3d$ peaks into four components, but the reference data on $\text{As}_2\text{S}_2\text{Se}$ and As_2SSe_2 are not currently available. Here we use two reference environments to show the As environment transition. No evidence of As–As (at a lower binding energy than that of AsSe_3) can be found based on peak-fitting results.

Figure 5 shows the $\text{S}2p$ peak deconvolution of $\text{As}_{40}\text{S}_{60-x}\text{Se}_x$ glasses. While most of the S would form As–S–As bonds, it is possible for some S to form wrong bonds As–S–S–As. From Raman, we observed low but measurable

signal for S–S bonds in As_2S_3 bulk glasses. XPS data analysis of $\text{As}_{40}\text{S}_{60-x}\text{Se}_x$ glasses also show two S environments in As_2S_3 , one as the dominant As–S–As, the other as As–S–S. In the Se-containing $\text{As}_{40}\text{S}_{60-x}\text{Se}_x$ glasses (samples 2–5 in Fig. 1), only one S environment is found. It is assigned to As–S–As species, and a small ($\sim 0.05\text{ eV}$) yet systematic increase is found in S binding energy when the Se content increases. We believe this small change of S binding energy is due to the systematic change of As–S–As bonds, associated with the introduction of Se into the As_2S_3 network and the corresponding occurrence of mixed pyramidal units. It might be expected that in such mixed units As–S bonds are stretched with Se addition (bond length longer than that in As_2S_3), and As–Se bonds are contracted with S addition (bond length shorter than that of As_2Se_3), so the S binding energy in a mixed pyramidal unit would be expected to be slightly higher than in an AsS_3 unit. Similarly, the Se binding energy in mixed pyramidal units should be slightly lower than in the AsSe_3 unit, which is observed in $\text{Se}3d$ peak deconvolution results (Fig. 4), as well as a small yet systematic decrease of the Se binding energy of the As–Se–As environment, due to the same reason.

As with S, most Se form As–Se–As bonds. The difference between S and Se environments is that while S is found in two environments only in As_2S_3 composition, Se is found in two environments in all stoichiometric compositions. While most of Se is assigned to Se in pyramidal unit As–Se–As, the second environment is explained in terms of As–Se–Ch (As–Se–S–As or As–Se–Se, depending on the composition), present in low concentrations. Because there is no evidence of the existence of As–S–Se–As in $\text{S}2p$ deconvolution results, we assume that As–Se–Ch is mainly As–Se–Se bonds in the stoichiometric series.

It is not surprising to see a limited amount of Ch–Ch bonds in stoichiometric As–S–Se glasses, due to the disordered nature of the glass system. The observation that when Se is present in the glass system, S stays in pyramidal units and Se forms Se–Se bonds is well consistent with our earlier conclusion.⁴

However, there is one concern about the $\text{As}3d$ deconvolution results: one might expect As–As bonds corresponding to the Ch–Ch bonds in the stoichiometric compositions, most likely in structures such as As–AsCh₂, but we do not find such evidence in $\text{As}3d$ deconvolution results. One possible explanation is that the environment change for As from AsCh_3 to As–AsCh₂ is for one third of the neighbors, but for the Ch a change from As–Ch–As to As–Ch–Ch is for one half of the environments, so the binding energy change is less noticeable. An EDS composition study on these glasses is ongoing to verify the composition of these glasses, again to see if there is any possible change in the glass melting-quenching process that would cause these glasses to be slightly chalcogen-rich. As mentioned in the sample preparation, the compositions of these samples were verified after glass formation to have an error around 1%.

B. $\text{As}_{24}\text{S}_{76-x}\text{Se}_x$ glasses ($x=0, 19, 38, 57, 76$)

1. Raman results

In chalcogen-rich binary systems $\text{As}_x\text{Ch}_{1-x}$ ($\text{Ch}=\text{S}, \text{Se}$, and $x < 0.4$), the molecular structure has been widely accepted as a random network of chalcogen chain fragments cross-linked by pyramidal $\text{AsCh}_{3/2}$ units.^{18,19}

According to previous Raman studies,^{76,93} the Raman-active vibrations at 345 cm^{-1} observed in As_2S_3 and at 230 cm^{-1} observed in As_2Se_3 are due to an intermolecular mode resulting from an antisymmetric As–S–As and As–Se–As stretching vibration, respectively. Two bands at 434 and 474 cm^{-1} have been reported in liquid sulfur as bond stretching of S_8 rings.⁹⁴ The band at around 255 cm^{-1} is attributed to Se–Se bond vibrations.^{95,4} In pure amorphous Se, an intense band occurs at 250 cm^{-1} with a small shoulder at 235 cm^{-1} . The band at 250 cm^{-1} has been attributed by Lucovsky⁹⁰ to stretching vibrations of “meandering” Se chains, while the small shoulder at 235 cm^{-1} (typical of crystalline trigonal Se) has been associated with helical chains.

Figure 7 shows the peak deconvolution of the Raman results for $\text{As}_{24}\text{S}_{76-x}\text{Se}_x$ glasses, using the same peak components. Comparing the Raman results for the chalcogen-rich glasses with the stoichiometric ternary compounds $\text{As}_{40}\text{S}_{60-x}\text{Se}_x$, it is evident that the chalcogen-chalcogen bonds, such as S–S and Se–Se or S–Se, exist in the chalcogen-rich As–S–Se glass system.

The evidences of the S–S chain (494 cm^{-1}) and S ring-like (474 cm^{-1}) structures are clearly visible in the Raman spectra of $\text{As}_{24}\text{S}_{76}$ and $\text{As}_{24}\text{S}_{57}\text{Se}_{19}$, while the evidence of Se–Se bonds can be observed in Se-containing glasses. For instance, in $\text{As}_{24}\text{Se}_{76}$, the peak component around 257 cm^{-1} has been shown in two peaks: one is assigned to $\text{AsS}_{3-n}\text{Se}_n$ pyramids (shown in solid line), and its intensity is chosen so that its relative intensity to the AsSe_3 (227 cm^{-1}) component is the same with that in $\text{As}_{40}\text{Se}_{60}$; and the other is shown in dashed line, which is assigned to Se–Se vibration. Similarly, the Se–Se vibration is evident in all $\text{As}_{24}\text{S}_{76-x}\text{Se}_x$ ternary glasses.

While the formation of Se–Se is evident from the 257 cm^{-1} vibration, and S–S from the 474 cm^{-1} and 494 cm^{-1} vibration, the S–Se bond⁹⁶ is indicated by the vibration at 355 cm^{-1} , which is used in $\text{As}_{24}\text{S}_{38}\text{Se}_{38}$ (only) as a peak component for peak fitting.

It can be seen that the S–S bonds reduce rapidly with a decrease of S content, and disappear at $\text{S}=38$ at. %. Se–Se bonds reduce more slowly in content with a similar decrease in Se content; for example, there are still a substantial number at $\text{Se}=38$ at. %. The relative concentration difference between Se–Se and S–S bonds in $\text{As}_{24}\text{S}_{38}\text{Se}_{38}$ is striking; we can confidently suggest that it is the S atom which remains in the pyramidal AsCh_3 units, while the Se tends to form homopolar Se–Se or heteropolar S–Se bonds.

In $\text{As}_{24}\text{S}_{76}$, two bands at 365 and 465 cm^{-1} are observed, both indicative of the As_2S_5 species present in the structure. With increasing Se content, there is a slight shift of the peak of the As–S-related broad band toward higher frequencies. This observation may be related to the contribution of S–Se bands, but we also observe a similar trend in the stoichiomet-

ric system (to a lesser extent), whose reason is not yet clear. The peak position shift (towards higher frequencies) of As–Se-related bonds with increasing S content can be explained in terms of a decrease in the effective mass of the vibrational mode.

2. XPS results

Figures 8, 9, and 10 show the peak deconvolution of the XPS results of $\text{As}3d$, $\text{Se}3d$, and $\text{S}2p$ for the $\text{As}_{24}\text{S}_{76-x}\text{Se}_x$ series. In Fig. 8, $\text{As}3d$ peaks are deconvolved into two components, AsS_3 and AsSe_3 . In chalcogen-rich glasses, there is very little chance of forming As–As bonds, so we can safely assume that in these glasses As atoms are found in (pure or mixed) AsCh_3 pyramidal units. Fitting results show that As species mainly remain connected with S to form AsS_3 pyramidal units, and Se joins the unit to form mixed pyramidal only when there is no sufficient S (at $\text{As}_{24}\text{S}_{19}\text{Se}_{57}$).

According to $\text{S}2p$ and $\text{Se}3p$ fitting results (Fig. 10), three S environments are found in $\text{As}_{24}\text{S}_{76}$, which are assigned to As–S–As, As–S–S–As, and As–S–S–S–As. For $\text{As}_{24}\text{S}_{57}\text{Se}_{19}$, there are also three S environments, As–S–As, As–S–S–As, and As–S–S–Se–As. In $\text{As}_{24}\text{S}_{38}\text{Se}_{38}$, two S environments are found, As–S–As and As–S–Se; similar is the case for $\text{As}_{24}\text{S}_{19}\text{Se}_{57}$. In chalcogen-rich environments, As–Ch–Ch–As(Ch)–links can have many different combinations and link orders, it is possible that there are more than one species around certain experimentally distinct binding energy values. The fitting results clearly show that there are Ch–Ch bonds in the chalcogen-rich composition, and Se has a bigger tendency to stay in the chain. Similar to the stoichiometric $\text{As}_{40}(\text{S}, \text{Se})_{60}$ series, the sulfur binding energy in As–S–As is slightly higher in Se-rich composition, which could be due to the same reason for the stoichiometric series.

For $\text{Se}3d$ spectra in chalcogen-rich glasses, peak deconvolution results (Fig. 9) show three Se environments, As–Se–As, As–Se–Se, and As–S–Se–Se. It is possible that the binding energy of Se–Se–Se is located very close to that of As–Se–Se, so that it is difficult to differentiate them.

One important observation, while evaluating the valence band structure, is the intensity change of the two bands located at 2.5 and 5.5 eV . In the elemental Se valence band, the peak at 5.5 eV is associated with the bonding p band ($4p$) and the peak at 2.5 eV with the lone-pair orbital.⁹⁷ These two features in the valence band of $\text{As}_{24}\text{S}_x\text{Se}_{76-x}$ glass indicate that considerable number of Se–Se homopolar bonds exists in chalcogen-rich As–S–Se compositions, consistent with previously discussed Raman results.

A comparison of the $\text{As}_{40}\text{S}_{60-x}\text{Se}_x$ series (stoichiometric compositions) and the $\text{As}_{24}\text{S}_{76-x}\text{Se}_x$ series (chalcogen-rich compositions) shows a clear difference around 2.5 eV (the bonding $4p$ bond), which indicates more Se–Se homopolar bonds in chalcogen-rich compositions and supports previously proposed structural reason related to chalcogen-rich composition having high optical nonlinearities.⁴

3. EXAFS results

EXAFS results showed that the average bond length around As was almost the same for $\text{As}_{24}\text{S}_{57}\text{Se}_{19}$ (2.3 \AA) and

$\text{As}_{24}\text{S}_{38}\text{Se}_{38}$ (2.29 Å), but larger for $\text{As}_{24}\text{S}_{19}\text{Se}_{57}$ (2.34 Å). This further indicates that for $\text{As}_{24}\text{S}_{57}\text{Se}_{19}$ and $\text{As}_{24}\text{S}_{38}\text{Se}_{38}$, there is only a minimal difference in the As environment, but for $\text{As}_{24}\text{S}_{19}\text{Se}_{57}$, there is a large change in the bond length. Considering the ideal covalent bond distance, $R_{\text{As-Se}}$ (2.38 Å) and $R_{\text{As-S}}$ (2.25 Å),^{69,70} these results suggest that the nearest neighbor of As in S-rich or S/Se=1 compositions is mainly S, with Se becoming the nearest neighbor only after S/Se is less than 1.0. Because our glass samples are chalcogen-rich, the As-As bond is not considered, as its concentration is expected to be negligible.

EXAFS data-fitting results showed that As has a coordination number of 3–4 in chalcogen-rich As–S–Se. S is preferred to be the near neighbors of As when there are plenty S, such as in $\text{As}_{24}\text{S}_{38}\text{Se}_{38}$ and $\text{As}_{24}\text{S}_{57}\text{Se}_{19}$. Only when the S amount is too low to meet the coordination requirement of As will Se also become a nearest neighbor of As (in the case $\text{As}_{24}\text{S}_{19}\text{Se}_{57}$). This agrees with both XPS and Raman that S mainly forms $\text{AsS}_{3/2}$ units, and Se will stay in the chain, along with any residual S atoms.

V. CONCLUSIONS

- (1) Raman bands at 200–280 and 280–400 cm^{-1} indicate that in $\text{As}_{40}\text{S}_{60-x}\text{Se}_x$ glasses, the main structures are AsCh_3 pyramidal units and the peak shift of As–S–As vibrations provides further evidence for mixed pyramidal units.
- (2) XPS results show the gradual change of As environments, which is consistent with the Raman finding of mixed pyramidal units.
- (3) XPS data also show that there are some, although in limited amount, chalcogen-chalcogen bonds in the stoichiometric compositions, S–S (Se–Se) in As_2S_3 (As_2Se_3) binary glasses and only Se–Se in As–S–Se ternary glasses, which indicates that Se has a bigger tendency to form chalcogen-chalcogen bonds.
- (4) The lack of XPS evidence of As–As bonds is possibly due to the smaller change in the As environment observed by XPS; further research is needed to provide evidence of As–As bonds.
- (5) For chalcogen-rich As–S–Se glasses, Raman results show that the molecular structure, similar to the binary glass system $\text{As}_x\text{Ch}_{1-x}$, consists of a network of chalcogen chain fragments cross-linked by pyramidal AsCh_3 units. The presence of the substantial amount of S–S, S–Se, and Se–Se bonds is evident through different Raman vibrations.
- (6) Supporting the finding in stoichiometric composition, in chalcogen-rich system, there are clear evidences to show that when there is extra chalcogen in the system, Se atoms tend to form chalcogen-chalcogen chains, while S prefers to stay in the AsCh_3 pyramidal units.

Finally, we conclude that complementary techniques lead to a constant understanding of structure and electronic properties, which allows us to better understand the attractive optical properties of these glasses.

ACKNOWLEDGMENTS

We would like to thank the National Science Foundation for supporting this work through NSF Grant Nos. DMR-9974129 and DMR-0312081. Our appreciation also extends to the Materials Characterization Facility at the University of Central Florida (UCF), the Physics Department at UCF, Zettlemoyer Center for Surface Studies at Lehigh University, and Stanford Synchrotron Radiation Laboratory for their hospitality and staff support.

- ¹R. Frerichs, Phys. Rev. **78**, 643 (1950).
- ²R. Frerichs, J. Opt. Soc. Am. **43**, 1153 (1953).
- ³A. R. Hilton, J. Non-Cryst. Solids **2**, 28 (1970).
- ⁴T. Cardinal, K. A. Richardson, H. Shim, A. Schulte, R. Beatty, K. Le Foulgoc, C. Meneghini, J. F. Viens, and A. Villeneuve, J. Non-Cryst. Solids **256–257**, 353 (1999).
- ⁵D. W. Hall, M. A. Newhouse, N. F. Borrelli, W. H. Dumbaugh, and D. L. Weidman, Appl. Phys. Lett. **54**, 1293 (1989).
- ⁶O. M. Efimov, L. B. Glebov, K. A. Richardson, E. Van Stryland, T. Cardinal, S. H. Park, M. Couzi, and J. L. Bruneel, Opt. Mater. **17**, 379 (2001).
- ⁷A. V. Stronski, M. Vlcek, A. Sklenar, P. E. Shepeljavi, S. A. Kostyukevich, and T. Wagner, J. Non-Cryst. Solids **266–269**, 973 (2000).
- ⁸M. Asobe, K. Suzuki, T. Kanamori, and K. Kubodera, Appl. Phys. Lett. **60**, 1153 (1992).
- ⁹A. Saliminia, A. Villeneuve, T. V. Galstyan, S. LaRoche, and K. Richardson, J. Lightwave Technol. **17**, 837 (1999).
- ¹⁰J. M. Harbold, F. O. Ilday, F. W. Wise, J. S. Sanghera, I. D. Aggarwal, and B. G. Aitken, Proc. SPIE **5061**, 143 (2003).
- ¹¹W. E. Morgan and J. R. Van Wazer, J. Phys. Chem. **77**, 964 (1973).
- ¹²J. F. Moulder, W. F. Sticker, P. E. Sobol, and K. D. Bomben, *Handbook of X-Ray Photoelectron Spectroscopy* (Perkin-Elmer, Eden Prairie, Minnesota, 1992).
- ¹³A. V. Kolobov, H. Oyanagi, and K. Tanaka, Phys. Rev. Lett. **87**, 145502 (2001).
- ¹⁴A. V. Kolobov, H. Oyanagi, K. Tanaka, and K. Tanaka, Phys. Rev. B **55**, 726 (1997).
- ¹⁵G. Chen, H. Jain, S. Khalid, J. Li, D. A. Drabold, and S. R. Elliott, Solid State Commun. **120**, 149 (2001).
- ¹⁶J. S. Sanghera, L. B. Shaw, and I. D. Aggarwal, C. R. Chim. **5**, 873 (2002).
- ¹⁷M. A. Popescu, *Non-Crystalline Chalcogenides* (Kluwer Academic, Boston, 2000), p. 27.
- ¹⁸A. T. Ward, J. Phys. Chem. **72**, 4133 (1968).
- ¹⁹P. J. S. Ewen, M. J. Sik, and A. E. Owen, Solid State Commun. **33**, 1067 (1980).
- ²⁰S. Onari, K. Matsuishi, and T. Arai, J. Non-Cryst. Solids **74**, 67 (1985).
- ²¹M. Malyj, G. P. Espinosa, and J. E. Griffiths, Solid State Commun. **62**, 671 (1987).
- ²²M. Frumar, Z. Polak, and Z. Cernosek, J. Non-Cryst. Solids **256–257**, 105 (1999).
- ²³V. Kovanda, M. Vlcek, and H. Jain, J. Non-Cryst. Solids **326–327**, 88 (2003).
- ²⁴A. Schulte and K. Richardson, in *Recent Research Developments in Non-Crystalline Solids 2*, edited by M. Kawasaki, N. Ashgriz, and R. Anthony (Transworld Research Network, Trivandrum, 2002, Vol. 1, 143–158).
- ²⁵C. Rivero, A. Schulte, and K. Richardson, Ceram. Trans. **126**, 79 (2002).
- ²⁶R. J. Nemanich, G. A. N. Connell, T. M. Hayes, and R. A. Street, Phys. Rev. B **18**, 6900 (1978).
- ²⁷A. Schulte, C. Rivero, K. Richardson, K. Turcotte, V. Hamel, A. Villeneuve, T. Galstian, and R. Vallee, Opt. Commun. **198**, 125 (2001).
- ²⁸A. Gheorghiu, I. Lampre, S. Dupont, C. Senemaud, M. A. El Idrissi Raghni, P. E. Lippens, and J. Olivier-Fourcade, J. Alloys Compd. **228**, 143 (1995).
- ²⁹E. P. Domashevskaya, V. V. Gorbachev, V. A. Terekhov, V. M. Kashkarov, E. V. Panfilova, and A. V. Shchukarev, J. Electron Spectrosc. Relat. Phenom. **114–116**, 901 (2001).
- ³⁰L. Jiang, A. G. Fitzgerald, M. J. Rose, K. Christova, and V. Pamukchieva, J. Non-Cryst. Solids **297**, 13 (2002).
- ³¹M. Bruns, H. Klewe-Nebenius, G. Pfennig, E. Bychkov, and H. J. Ache, Surf. Coat. Technol. **97**, 707 (1997).

- ³²J. S. Berkes, S. W. Ing, Jr., and W. J. Hillegas, *J. Appl. Phys.* **42**, 4908 (1971).
- ³³A. V. Kolobov, *J. Non-Cryst. Solids* **164–166**, 1159 (1993).
- ³⁴A. V. Kolobov, J. P. S. Badyal, and R. M. Lambert, *Surf. Sci.* **222**, L819 (1989).
- ³⁵T. Kitahara and T. Arai, *Jpn. J. Appl. Phys.* **18**, 1635 (1979).
- ³⁶K. Antoine, J. Li, D. A. Drabold, H. Jain, M. Vlcek, and A. C. Miller, *J. Non-Cryst. Solids* **326–327**, 248 (2003).
- ³⁷H. Jain, S. Krishnaswami, A. C. Miller, P. Krcemer, S. R. Elliott, and M. Vlcek, *J. Non-Cryst. Solids* **274**, 115 (2000).
- ³⁸S. Seal, K. A. Richardson, C. Lopez, A. Graham, D. K. Verma, A. Salimina, T. Galstian, and A. Villeneuve, *Phys. Chem. Glasses* **43**, 59 (2002).
- ³⁹S. Seal, K. A. Richardson, W. Li, C. Lopez, A. Schulte, A. Graham, and C. Rivero, *Corrosion (Houston)* **59**, 139 (2003).
- ⁴⁰J. M. Durand, J. Olivier-Fourcade, J. C. Jumas, M. Womes, and P. Parent, *J. Mater. Sci.* **32**, 4679 (1997).
- ⁴¹J. M. Durand, P. E. Lippens, J. Olivier-Fourcade, J. C. Jumas, and M. Womes, *J. Non-Cryst. Solids* **194**, 109 (1996).
- ⁴²J. M. Durand, P. E. Lippens, J. Olivier-Fourcade, and J. C. Jumas, *J. Non-Cryst. Solids* **192–193**, 364 (1995).
- ⁴³G. Pfeiffer, J. J. Rehr, and D. E. Sayers, *Phys. Rev. B* **51**, 804 (1995).
- ⁴⁴C. Y. Yang, M. A. Paesler, and D. E. Sayers, *Phys. Rev. B* **39**, 10342 (1989).
- ⁴⁵Y. Yang, M. A. Paesler, and D. E. Sayers, *Phys. Rev. B* **36**, 9160 (1987).
- ⁴⁶A. V. Kolobov, K. Tanaka, and H. Oyanagi, *Phys. Solid State* **39**, 64 (1997).
- ⁴⁷A. M. Flank, D. Bazin, H. Dexpert, P. Lagarde, C. Hervo, and J. Y. Barraud, *J. Non-Cryst. Solids* **91**, 306 (1987).
- ⁴⁸P. Armand, A. Ibanez, and E. Philippot, *Nucl. Instrum. Methods Phys. Res. B* **97**, 176 (1995).
- ⁴⁹V. Mastelaro, S. Benazeth, and H. Dexpert, *J. Non-Cryst. Solids* **185**, 274 (1995).
- ⁵⁰D. G. Georgiev, P. Boolchand, and M. Micoulaut, *Phys. Rev. B* **62**, R9228 (2000).
- ⁵¹L. G. Protasova, P. I. Buler, and S. A. Subbotina, *Inorg. Mater. (USSR)* **25**, 659 (1989).
- ⁵²C. Y. Yang, M. A. Paesler, and D. E. Sayers, *Phys. Rev. B* **36**, 980 (1987).
- ⁵³W. Zhou, M. A. Paesler, and D. E. Sayers, *Phys. Rev. B* **43**, 11920 (1989).
- ⁵⁴J. M. Lee, G. Pfeiffer, M. A. Paesler, D. E. Sayers, and A. Fontaine, *J. Non-Cryst. Solids* **114**, 52 (1989).
- ⁵⁵J. M. Lee, M. A. Paesler, D. E. Sayers, and A. Fontaine, *J. Non-Cryst. Solids* **123**, 295 (1990).
- ⁵⁶A. V. Kolobov, H. Oyanagi, K. Tanaka, and K. Tanaka, *J. Lumin.* **66–67**, 174 (1996).
- ⁵⁷A. V. Kolobov, H. Oyanagi, K. Tanaka, and K. Tanaka, *J. Non-Cryst. Solids* **198–200**, 709 (1996).
- ⁵⁸J. Li and D. A. Drabold, *Phys. Rev. B* **64**, 104206 (2001).
- ⁵⁹J. Li, D. A. Drabold, S. Krishnaswami, G. Chen, and H. Jain, *Phys. Rev. Lett.* **88**, 046803 (2002).
- ⁶⁰G. Lucovsky and R. Martin, *J. Non-Cryst. Solids* **8–10**, 185 (1972).
- ⁶¹A. Schulte, *Appl. Spectrosc.* **46**, 891 (1992).
- ⁶²C. Rivero, thesis, University of Central Florida, 2001.
- ⁶³*GRAMS User's Guide* (Galactic Industries, Salem, NH, 1999).
- ⁶⁴D. A. Shirley, *Phys. Rev. B* **5**, 4709 (1972).
- ⁶⁵H. E. Bishop, *Surf. Interface Anal.* **3**, 272 (1981).
- ⁶⁶J. Vegh, *J. Electron Spectrosc. Relat. Phenom.* **46**, 411 (1988).
- ⁶⁷B.-K. Teo, in *EXAFS Spectroscopy: Techniques and Applications*, edited by B. K. Teo and D. C. Joy (Plenum, New York, 1981), p. 17.
- ⁶⁸D. Schiferl and C. S. Barrett, *J. Appl. Crystallogr.* **2**, 30 (1969).
- ⁶⁹A. C. Stergiou and P. J. Rentzeperis, *Z. Kristallogr.* **173**, 185 (1985).
- ⁷⁰D. J. E. Mullen and W. Nowaki, *Z. Kristallogr.* **136**, 48 (1972).
- ⁷¹A. L. Ankudinov and J. J. Rehr, *Phys. Rev. B* **56**, R1712 (1997).
- ⁷²<http://www-ssrl.slac.stanford.edu/exafspak.html>
- ⁷³E. Diemann, *Rev. Chim. Miner.* **16**, 237 (1979).
- ⁷⁴T. Wagner, S. O. Kasap, M. Vlcek, A. Sklenar, and A. Stronski, *J. Mater. Sci.* **33**, 5581 (1998).
- ⁷⁵D. W. Scott, J. P. McCullough, and F. H. Kruse, *J. Mol. Spectrosc.* **13**, 313 (1964).
- ⁷⁶P. Nagels, *Semiconductors* **32**, 855 (1998).
- ⁷⁷A. Feltz and G. Pfaff, *J. Non-Cryst. Solids* **77–78**, 1137 (1985).
- ⁷⁸G. Lucovsky, *Phys. Rev. B* **6**, 1480 (1972).
- ⁷⁹P. Boolchand, D. G. Georgiev, T. Qu, F. Wang, L. Cai, and S. Chakravaty, *C. R. Chim.* **5**, 713 (2002).
- ⁸⁰M. Frumar, J. Jedelsky, B. Frumarova, T. Wagner, and M. Hrdlicka, *J. Non-Cryst. Solids* **326–327**, 399 (2003).
- ⁸¹V. I. Mikla, *J. Phys.: Condens. Matter* **8**, 429 (1996).
- ⁸²A. Bertoluzza, C. Fagnano, P. Monti, and G. Semerano, *J. Non-Cryst. Solids* **29**, 49 (1978).
- ⁸³J. Schottmiller, M. Tabak, G. Lucovsky, and A. Ward, *J. Non-Cryst. Solids* **4**, 80 (1970).
- ⁸⁴T. Mori, S. Onari, and T. Arai, *Jpn. J. Appl. Phys.* **19**, 1027 (1980).
- ⁸⁵V. I. Mikla, A. A. Baganich, A. P. Sokolov, D. G. Semak, and A. P. Shebanin, *Sov. Phys. Solid State* **34**, 1433 (1992).
- ⁸⁶V. I. Mikla, A. A. Baganich, A. P. Sokolov, and A. P. Shebanin, *Phys. Status Solidi B* **175**, 281 (1993).
- ⁸⁷J. A. Freitas, Jr., U. Strom, and D. J. Treacy, *J. Non-Cryst. Solids* **59–60**, 875 (1983).
- ⁸⁸S. Onari, H. Saegusa, T. Mori, and T. Arai, *J. Non-Cryst. Solids* **59–60**, 871 (1983).
- ⁸⁹R. Zallen, M. L. Slade, and A. T. Ward, *Phys. Rev. B* **3**, 4257 (1971).
- ⁹⁰G. Lucovsky, in *The Physics of Selenium and Tellurium*, edited by E. Gerlach and P. Grosse (Springer, Berlin, 1979), p. 210.
- ⁹¹M. L. Slade and R. Zallen, *Solid State Commun.* **30**, 357 (1979).
- ⁹²D. J. Treacy, U. Strom, P. B. Klein, P. C. Taylor, and T. P. Martin, *J. Non-Cryst. Solids* **35–36**, 1035 (1980).
- ⁹³J. A. Freitas, Jr., U. Strom, and D. J. Treacy, *J. Non-Cryst. Solids* **59–60**, 875 (1983).
- ⁹⁴K. Hattori and H. Kawamura, *J. Non-Cryst. Solids* **59–60**, 1063 (1983).
- ⁹⁵A. Kolobov, H. Oyanagi, A. Roy, and K. Tanaka, *J. Non-Cryst. Solids* **227–230**, 710 (1998).
- ⁹⁶A. T. Ward, *J. Phys. Chem.* **74**, 4110 (1970).
- ⁹⁷N. J. Shevchik, M. Cardona, and J. Tejada, *Phys. Rev. B* **8**, 2833 (1973).